Nonequilibrium Phase Winding and Its Breakdown at a Chiral Interface

H. R. Brand[1] and P. E. Cladis[2]

[1]*Theoretische Physik III, Universität Bayreuth, D 95440 Bayreuth, Federal Republic of Germany*
[2]*AT&T Bell Laboratories, Murray Hill, New Jersey 07974*

(Received 27 September 1993)

We describe a nonequilibrium phase winding of the liquid-crystal director at a flat cholesteric-isotropic interface. The physical origin of the driving force is a symmetry-allowed coupling between an equilibrium helix structure and gradients in impurity concentration set up at an interface forced to move by displacing the sample in a temperature gradient. We interpret these observations to evaluate the coupling constant: $|\nu_c| = 3 \times 10^{-4}$ dyn/cm. A second transition is observed at higher displacement speeds to an orientationally disordered state.

PACS numbers: 61.30.−v, 05.70.Ln, 47.20.−k

The study of patterns formed at liquid-solid interfaces moving in a temperature gradient (directional solidification) is a rapidly growing area in the field of pattern forming nonequilibrium systems [1]. Recently, focus has changed to phase transitions involving broken continuous rotational symmetry [2–5]. Previously, we showed [6] that when there is a combined broken continuous rotational and translational symmetry, all the cellular nonequilibrium states have at least one frequency. As a secondary instability, we observed a breathing mode arising from competition between an equilibrium and a nonequilibrium length scale [6]. Very recently, we investigated [7] patterns obtained at a traveling interface between a state with a chirality-induced defect lattice (twist grain boundary phase [8]) and another liquid-crystalline state.

Here we report that, even behind a flat interface, at sufficiently high temperature gradients and sufficiently large pulling speeds, there are nonequilibrium states characterized by long spatial correlations of the director phase that winds at the interface at a fixed frequency: the *forced phase winding* regime. At even larger pulling speeds and/or temperature gradients, spatial correlations of the phase winding decrease, eventually leading to a nonequilibrium state disordered in both space and time: an *orientational glass* whose disordered, nonequilibrium character is revealed most clearly as the region behind the interface anneals.

We use the same experimental setup as in our previous studies on the cholesteric-isotropic interface [6,9]. The temperature gradient $\mathbf{G}$ and the sample displacement velocity (*pulling speed*) $\mathbf{v}$ are both $\parallel \hat{\mathbf{z}}$. The material used in this study is a mixture of the nematic liquid crystal 8CB (cyano-octylbiphenyl) and the chiral impurity $C15$ (cyano-methyl-butoxybiphenyl) with a concentration $c_\infty = 9\%$ by weight. The nematic phase has long range orientational order along a direction characterized by a unit vector, the director, $\hat{\mathbf{n}}$, that does not distinguish between head and tail [10].

We prepare our samples with the cholesteric phase [10] at equilibrium such that $\hat{\mathbf{n}}$ rotates uniformly above a twist axis, $\mathbf{q}_0$, with $\mathbf{q}_0 \perp \hat{\mathbf{n}}$ and $\mathbf{q}_0 \parallel \hat{\mathbf{y}}$. The director is aligned $\parallel \hat{\mathbf{z}}$ at the top and bottom surfaces of the samples that are observed with an optical microscope along the direction perpendicular to these surfaces ($\hat{\mathbf{y}}$). In our mixture, the pitch, $p_0 = 2\pi/q_0$, the distance for a 2π rotation of $\hat{\mathbf{n}}$, is $p_0 = 38.5$ μm. The results presented here have been obtained for three different temperature gradients G ($G = 15$, 30, and 45 K/cm), and for three different sample thicknesses d ($d = 37$, 63, and 80 μm).

In Ref. [6], we note that as $v \to v_c^u$ (v_c^u is the upper critical speed for the stability of cellular patterns), the pattern wavelength decreases to p_0. Although when $v > v_c^u \sim 80$ μm/s and $G = 7.5$ K/cm, the interface is flat, novel phenomena appear that seem to have no analog in systems studied so far in directional growth of nonchiral systems without macroscopic equilibrium length scales such as p_0. The flat interface in our system shows a spatially coherent phase winding enforced by director rotation at the interface (forced phase winding, Fig. 1). The pattern in Fig. 1 shows a large coherence length both parallel and perpendicular to the interface.

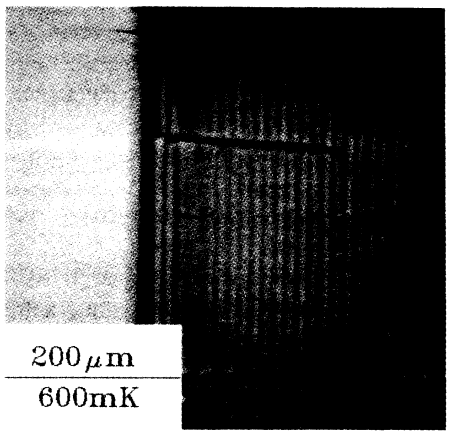

FIG. 1. Pattern behind flat interface for $d = 63$ μm, $v = 40$ μm/s, and $G = 30$ K/cm. The isotropic liquid is the featureless region to the left and the regular forced phase winding with large coherence length perpendicular to the interface is to the right. The lines perpendicular to the interface are localized regions with an apparent phase mismatch of the director.

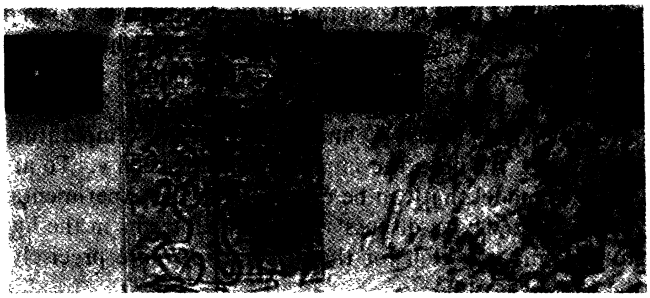

a b

FIG. 2. Orientational glass patterns behind the flat interface in a constant temperature gradient. Higher temperatures are to the left. (a) Growing the orientational glass state at (a) $v=70$ μm/s $\|\mathbf{G}$. (b) Defect structures observed as the orientational glass anneals in the temperature gradient during directional melting at $v=70$ μm/s. Sample thickness, $d=80$ μm, temperature gradient, $G=45$ K/cm. The arrow in the black box gives the direction of motion of the interface, which is outside the field of view in (b).

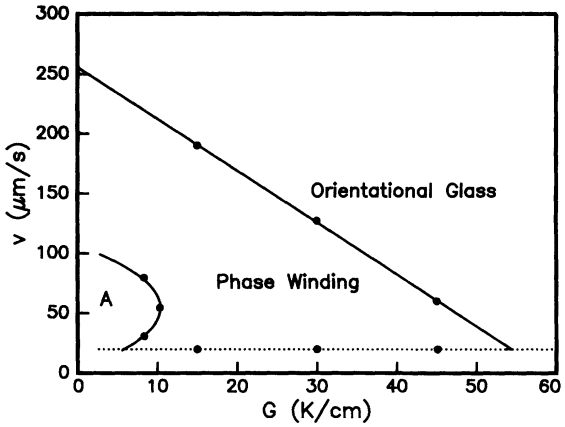

FIG. 3. Schematic of the phase diagram obtained in the velocity-temperature gradient (v-G) plane. Time-dependent cellular patterns are only observed in a small area (A) of the phase diagram, while the orientational glass dominates. Below the dotted line coherent phase winding is not observed.

As the pulling speed v increases, the wavelength of the emerging pattern also increases, but the phase coherence across the interface decreases. Above another critical speed, v_G, at fixed temperature gradient, phase coherence is lost, leaving in its wake a disordered liquid-crystalline state [Fig. 2(a)]. That this disordered, frozen-in state is reminescent of a glassy state becomes clear by studying the relaxing defect structures as it anneals [Fig. 2(b)]: A high density of defects with completely irregular spatial arrangement is observed that anneal as a function of time, first, to a helix free nematiclike state and only on much longer time scales does a common cholesteric fingerprint texture [11] emerge that in turn relaxes to the rest state with $\mathbf{q}_0 \| \hat{\mathbf{y}}$. We call this state an orientational glass because the system does not have enough time to organize itself in the coherent fashion observed at equilibrium or at smaller pulling speeds: A quenched state results when time is insufficient to pass information about the orientational order across the interface over macroscopic distances.

This behavior is somewhat similar to that observed for nematic liquid-crystalline side-chain polymers with a glass transition close to the nematic-isotropic transition [12]. In these systems, while nematic order is detected on short length scales (e.g., by x rays), no macroscopic order is observed. The polymer backbone strongly disturbs long range orientational order so that only small nematic clusters can form.

In Fig. 3, we plot the phase diagram in the temperature gradient-(G) pulling speed (v) space. Figure 3 shows only a small area of phase space occupied by the time-dependent cellular patterns while the forced phase winding and, in particular, the orientational glass states dominate for sufficiently high pulling speeds and temperature gradients. This is a familiar feature of hydrodynamic instabilities. For sufficiently large values of the external stress parameters (for example, the applied temperature gradient in Bénard convection or the applied torque in the Taylor instability) mostly turbulent (disordered in space and time) patterns populate parameter space.

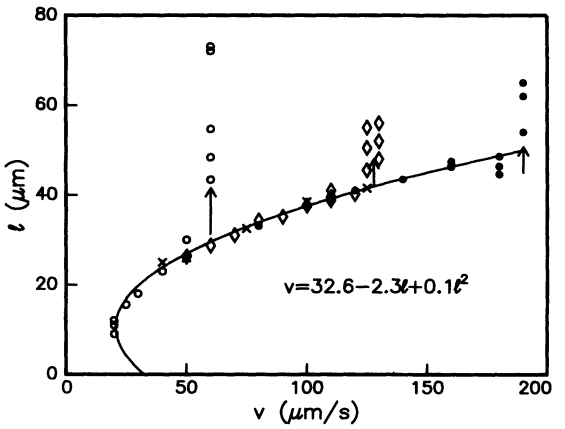

FIG. 4. Spacing l left behind the flat interface as a function of pulling speed v in the forced phase winding regime. The data obtained for three different sample thicknesses (●, ◇: 37 μm, ×: 63 μm, ○: 80 μm) and three different applied temperature gradients (●, ×: 15 K/cm, ◇: 30 K/cm, ○: 45 K/cm). The data on the 37 μm thick sample taken for two different temperature gradients show that the transition from forced phase winding to the orientational glass state depends on the applied temperature gradient and not on sample thickness. The data for the 63 μm thick sample are plotted to underscore the universal aspects of l vs v in the forced phase winding regime. In the immediate vicinity of the transition to the orientational glass state the data are time dependent. The band of lengths shown above the universal curve (solid line) is representative of the observed temporal variations. Phase coherence is lost in the orientational glass state and the band of length scales [see Fig. 2(a)] broadens with distance from the transition.

In Fig. 4, we plot the observed wavelength l of the pattern created at the flat interface in the forced phase winding regime as a function of pulling speed v for various sample thickness and temperature gradients. Figure 4 shows that all measurements in the forced phase winding regime fall on a universal curve that can be fitted to a parabolic shape (solid line). Inspecting Fig. 4, we conclude that we have a transcritical [13] bifurcation for the observed wavelength with the pulling speed v as the bifurcation parameter. That the pulling speed is the relevant bifurcation parameter for the cholesteric-isotropic interface was already clear from studying the cellular regime in this system [6].

The breakdown of the forced phase winding regime, and thus the onset of the orientational glass state, is marked in Fig. 4 with vertical arrows. While v_G, the pulling speed for this transition, does not depend on sample thickness (provided sample thickness is large enough to confine the influence of the surface treatment to boundary layers so that the director can rotate freely in the bulk of the sample), it does depend on the applied temperature gradient. In samples much thinner than the pitch, boundary layers heavily influence all patterns observed at the cholesteric-isotropic interface.

We now propose a macroscopic model that gives to a good approximation the relation between the observed wavelength and pulling speed shown in Fig. 4.

The observed director rotation about an axis $\|\mathbf{G}$ in the force phase winding regime is reminiscent of the Lehmann [14] effect [10,15] with free boundaries. In this effect, one considers the influence of an external temperature gradient applied parallel to the helical axis, $(\hat{\mathbf{z}})$, of a freely suspended drop of cholesteric liquid crystal with the director orientation defined as $\phi(z)$ in planes perpendicular to the helix axis, with the sample surfaces at $z=0$ and $z=d$; and free boundary conditions, $d\phi/dz|_{z=0} = d\phi/dz|_{z=d} = q_0$. For this configuration, one expects [10] the director to rotate at a uniform rate so that

$$\phi = q_0 z + \frac{v_T}{\gamma_1}\frac{dT/dz}{T}t + \phi_0 , \tag{1}$$

where ϕ_0 is an arbitrary constant and t is time. γ_1 is the rotational viscosity [10] and T is temperature. Finally, v_T is the Lehmann coefficient in de Gennes' notation (where the subscript T stands for temperature) and may be either positive or negative. On the basis of a dimensional analysis, de Gennes suggests an estimate for $v_T(\mathrm{dyn/cm}) = xK_2q_0 \sim 2\times10^{-7}q_0$ with x a dimensionless number of order 1. After Lehmann's original observation [14], there has recently been one report of an analogous effect in a dc electric field [16] but there have been no other reports of an experimental study of the Lehmann effect in a uniform temperature gradient.

In our system, a cholesteric-isotropic interface moving in a constant temperature gradient, the situation is more complex than the idealized geometry of the classical Lehmann effect. First, the surface treatment of the top and bottom plate is such that the equilibrium configuration sets the helix axis perpendicular to the pulling direction and the temperature gradient. Second, besides the usual force of the classical Lehmann effect, the temperature gradient $\mathbf{G}$, we have the imposed pulling speed $\mathbf{v}$. To arrive at a model that can be compared to the experimental results (Fig. 4), we discuss separately all terms in the hydrodynamic equation for the director, or more precisely, the phase variation $\delta\phi$.

We assume that the phase rotates in the interface at a fixed rate and average the dynamic equation over phase changes of 2π. From the material derivative $\gamma_1 d\phi/dt$, we get two contributions that are replaced under this assumption: $\partial\phi/\partial t \rightarrow 2\pi/\tau$ with τ to be determined from experiment, and $\partial\phi/\partial z \rightarrow 2\pi/l$, where l is the spacing observed in the forced phase winding regime behind the interface.

The next term is the Lehmann term. For our experimental configuration, the dominant contribution comes from the impurity concentration gradient at the interface [17]. Assuming stationary conditions for the concentration field, we replace $v_c\partial_z c \rightarrow v_c v/D_I$, where v_c is the Lehmann coefficient for concentration. D_I is the coefficient of impurity diffusion [18], $D_I \sim 4\times10^{-7}$ cm^2/s, in the isotropic liquid at the interface.

Finally, we must consider the contribution from elastic torques. This is a complicated task in our geometry. Thus, we propose a simple order of magnitude argument for the elastic restoring force: $\beta K_2 q_0 2\pi/l$, where β is an additional dimensionless fit parameter expected to be of order unity. This expression has the right dimensions. It contains q_0, characteristic for a cholesteric phase, and the wave number $k=2\pi/l$ of the pattern observed in the forced phase winding regime that we also expect to influence the restoring force. The price we pay for this simplified analysis is an additional fit parameter, β.

Combining all the terms discussed and guided by our parabolic fit to Fig. 4, we expand the velocity field v as a quadratic polynomial in l. That this expansion is justified becomes clear when inspecting the numbers obtained from the fit to the experimental results. Neglecting effects of order 1%, within the error bar of our experiments, we get the final expression:

$$v = \frac{-v_c}{2\pi\gamma_1 D_I \tau} l^2 - \frac{1}{\tau} l + \beta D_0 q_0 . \tag{2}$$

Equation (2) contains three fit parameters: β, τ, and v_c. The value of D_I has been given above. All other parameters are known [6,19]. Taking these values, we obtain from the fit to the experimental data $\beta = 2.7$, $1/\tau = 2.3$ s^{-1}, and $v_c = -3\times10^{-4}$ dyn/cm.

As expected, β is of order unity. The value of $1/\tau$ is close to the elastic frequency ω_{el} (Ref. [6], $\omega_{el}/2\pi = D_0 q_0^2 \sim 2$ s^{-1}) and the value for the Lehmann coefficient, v_c coupling concentration gradients and the helix orienta-

tion, $v_c = -3\times10^{-4}$ dyn/cm, coincides remarkably well with the order of magnitude estimate [10].

We also note the similarity of the increase in the helix pitch of a cholesteric in a static magnetic field [10] above the threshold field H_c, and the dynamic increase observed here at the traveling cholesteric-isotropic interface. Replacing $\chi_a H_c^2/K_2$ in the expression for the threshold in the former case [10] by $v_c v_c/K_2 D_I$, we obtain for v_c: $v_c = 16$ μm/s, a value quite close to the threshold obtained for forced phase winding: $v_c \sim 19$ μm/s.

We have shown that even for a flat chiral interface, there is a frequency to wind the director at a moving interface that can generate in its wake patterns with well-defined wavelengths. At pulling speeds too fast to allow local phase information, ϕ, to propagate across the interface over macroscopic distances, an orientational glass results where disorder in space and time is frozen-in and revealed by observations of the annealing process. We presented a macroscopic model for the forced phase winding regime that agrees well with experimental results and is consistent with a transcritical bifurcation. From this model, we deduced, for the first time, the Lehmann coefficient v_c, a transport coefficient allowed by symmetry in systems with macroscopic chirality coupling the macroscopic director orientation to concentration gradients.

P.E.C. acknowledges receipt of a 1993 John Simon Guggenheim Fellowship. We also acknowledge partial support of this work through NATO CRG 890777.

[1] J. M. Flesselles, A. J. Simon, and A. Libchaber, Adv. Phys. **30**, 1 (1991), and references cited therein.

[2] P. Oswald, J. Bechhoefer, A. Libchaber, and F. Lequeux, Phys. Rev. A **36**, 5832 (1987).

[3] A. J. Simon, J. Bechhoefer, and A. Libchaber, Phys. Rev. Lett. **61**, 2574 (1988); J. Bechhoefer, A. J. Simon, A. Libchaber, and P. Oswald, Phys. Rev. A **40**, 2042 (1989).

[4] P. Oswald, J. Bechhoefer, and F. Melo, MRS Bull. **XVI**, No. 1, 38 (1991).

[5] P. Oswald, J. Phys. II (France) **1**, 571 (1991).

[6] P. E. Cladis, J. T. Gleeson, P. L. Finn, and H. R. Brand, Phys. Rev. Lett. **67**, 3239 (1991).

[7] P. E. Cladis, A. J. Slaney, J. W. Goodby, and H. R. Brand (to be published).

[8] S. R. Renn and T. C. Lubensky, Phys. Rev. A **38**, 2132 (1988).

[9] P. E. Cladis, J. T. Gleeson, and P. L. Finn, in *Defects, Patterns and Instabilities,* edited by D. Walgraef and N. M. Ghoniem (Kluwer Academic, Dordrecht, 1990).

[10] P. G. de Gennes, *Physics of Liquid Crystals* (Clarendon, Oxford, 1982), 3rd ed.

[11] P. E. Cladis and M. Kleman, Mol. Cryst. Liq. Cryst. **16**, 1 (1972).

[12] H. Finkelmann and D. Day, Makromol. Chem. **180**, 2269 (1979).

[13] P. Manneville, in *Dissipative Structures and Weak Turbulence* (Academic, New York, 1990), p. 160.

[14] O. Lehmann, Ann. Phys. (Leipzig) **2**, 649 (1900).

[15] H. R. Brand and H. Pleiner, Phys. Rev. A **37**, 2736 (1988).

[16] N. V. Madhusudana and R. Pratibha, Mol. Cryst. Liq. Cryst. Lett. **5**, 43 (1987).

[17] The thermal length $l_T \equiv \Delta T/G \sim 100$ μm $\gg l_D \sim 0.2$ μm.

[18] M. Hara, H. Takezoe, and A. Fukuda, Jpn. J. Appl. Phys. **25**, 1756 (1986).

[19] H. Kneppe, F. Schneider, and N. K. Sharma, J. Chem. Phys. **77**, 3203 (1982).

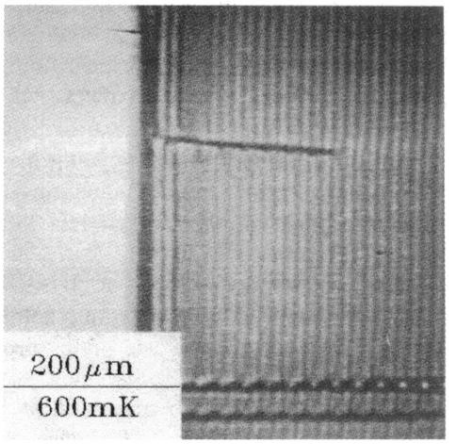

FIG. 1. Pattern behind flat interface for $d = 63$ μm, $v = 40$ μm/s, and $G = 30$ K/cm. The isotropic liquid is the featureless region to the left and the regular forced phase winding with large coherence length perpendicular to the interface is to the right. The lines perpendicular to the interface are localized regions with an apparent phase mismatch of the director.

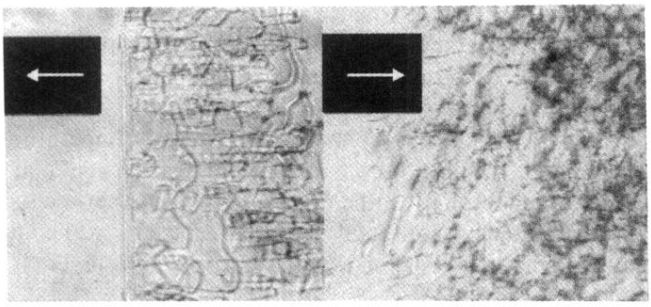

a b

FIG. 2. Orientational glass patterns behind the flat interface in a constant temperature gradient. Higher temperatures are to the left. (a) Growing the orientational glass state at (a) $v = 70$ μm/s $\|\mathbf{G}$. (b) Defect structures observed as the orientational glass anneals in the temperature gradient during directional melting at $v = 70$ μm/s. Sample thickness, $d = 80$ μm, temperature gradient, $G = 45$ K/cm. The arrow in the black box gives the direction of motion of the interface, which is outside the field of view in (b).